

# Empirical Modeling and Position Control of Single Pneumatic Artificial Muscle

Bitao Yao\*, Zude Zhou\*, Quan Liu\*\*, Qingsong Ai\*\*

\*School of Mechanical and Electronic Engineering, Wuhan University of Technology, Wuhan, China  
(e-mail: {bitaoyao, zudezhou}@whut.edu.cn)

\*\*School of Information Engineering, Wuhan University of Technology, Wuhan, China  
(e-mail: {quanliu, qingsongai}@whut.edu.cn)

**Abstract:** The model of pneumatic artificial muscles (PAMs) is the foundation of their control. Compared to theoretical model, empirical model is based on experiments and doesn't need accurate understanding of PAMs. Existing ones have not considered the history-dependence of hysteresis within PAMs which causes creep and deteriorates the controller behavior. In this paper, a novel synthetically empirical model of PAMs which consists of hysteresis element, viscous damping element, rubber elasticity element and contractile element in parallel is proposed. The accuracy of the empirical model is verified by experiments. This model is then applied into the position control of single PAM using fuzzy logic. To overcome the negative impact of hysteresis and to improve the response speed of the controller, the proposed model is then used to calculate an on-line feedforward voltage to the solenoid valve for compensation. In order to improve the robust of the controller, a self-organizing mechanism is introduced. Experimental results indicate that the proposed controller effectively alleviates the creep of PAM and improves in response speed and robustness while maintaining stability.

**Keywords:** Pneumatic artificial muscles (PAMs), Empirical modeling, Position control, Compensation, Fuzzy logic.

## 1. INTRODUCTION

PAMs are new type of actuators which possess advantages of high power/weight ratio, high power/volume ratio, light weighted and inherent compliance, and were popularized by an American physicist J.L. McKibben who employed PAMs in physical rehabilitation (Doumit et al., 2009). It is found that McKibben muscles show similar characteristics to biological muscles (Chou et al., 1996) and are suitable to be actuators for rehabilitation robot. The most generally used PAMs are the braided fiber-reinforced type based on McKibben muscle which consists of an rubber tube and an outer inextensible braided sheath with both ends sealed by caps (Chou et al., 1996; Shen et al., 2011). When the rubber tube is pressurized, its volume increases and the rubber tube is push against the outer braided sheath. Because the outer braided sheath is inextensible, the axial extension of the rubber tube is restricted and then expands in radius and gets shorten. If the McKibben muscle is coupled to a load, it will exert a contraction force. The PAMs studied in this paper are made by FESTO (as show in Fig. 1). FESTO PAMs are different from McKibben muscles as the rubber tube and the outer braided sheath are mixed together. However, both McKibben muscles and FESTO PAMs are braided fiber-reinforced type (Shen et al., 2011).



Fig. 1. FESTO PAM.

### 1.1 Modeling of PAMs

Though the advantages of PAMs, they have high non-linearity and time-variant properties due to the inherent characters of rubber tube, the compressibility of air and the friction between the tube and the sheath. Therefore, it is difficult to model the PAMs accurately.

Most of the models of PAMs are theoretical ones which are based on energy conservation. Many factors were considered to make corrections to ideal model derived from energy conservation, such as the thickness of rubber tube (Chou et al., 1996; Kothera et al., 2009), non-cylindrical geometric shape of PAMs (Tondou et al., 2000; Kothera et al., 2009), the distortion at the ends of PAM (Tsagarakis et al., 2000), elastic energy storage of rubber tube (Klute et al., 2000; Kothera et al., 2009; Zhong et al., 2014), the radial pressure loss due to rubber elasticity (Tsagarakis et al., 2000), the elasticity of outer braid (Kothera et al., 2009), the fiber braid friction (Zhong et al., 2014).

As it can be very hard to obtain the exact values of some parameters within theoretical models, some researchers obtain empirical models of PAMs based on experimental data. A three-element model which included contractile element, spring element, and damping element in parallel was proposed (Reynolds et al., 2003). In that model, the spring and damping element functions of pressure were determined by static perturbation method at constant pressure. The functions in dynamic condition were hypothesized to be the same as pertain to static condition. Some researchers

modeled PAM as a mechanical spring of variable stiffness which was the function of operational air pressure and the stretched length (Wickramatunge et al., 2013). Polynomial was also adopted to describe the dynamics of PAMs (Balasubramanian et al., 2007; Pujana-Arrese et al., 2010). However, these empirical models generally did not consider the history-dependence of hysteresis within PAMs.

Hysteresis means that the force or pressure during the contraction of PAM is higher than that during extension at the same contract ratio. Hysteresis is caused by coulomb friction between the tube and the sheath and between the braided threads (Chou et al., 1996; Tondu et al., 2000). The friction was velocity independent but history dependent. Maxwell-slip model, which was a lumped-parametric quasi-static model, was used to capture the friction and hysteresis in FESTO PAMs (Minh et al., 2011). Hysteresis was found to cause oscillation within PAMs (Minh et al., 2010).

### 1.2 Control of PAMs

As PAMs are actuators of high nonlinearity and time-variant properties, it is rather hard to control PAMs accurately. To overcome these difficulties, researchers have proposed various control strategies. Variable structure control (VSC) is a kind of model-based and self-adaptation control strategy which is robust to disturbance and uncertainties caused by nonlinearity and time-variant properties. Many researchers adopted VSC in the control of PAMs (Pujana-Arrese et al., 2010; Repperger et al., 1998; Carbonell et al., 2001; Xing et al., 2010; Shen et al., 2010; Rezoug et al., 2013). But VSC needs a relatively accurate model because it is difficult to design a stable controller with a model that includes too many uncertainties. Moreover, the control signal in VSC chatters during controlling and may stimulate unmodeled properties of system. This thus deteriorates the stability of VSC controller.

Nowadays, expert control methods are used widely in nonlinearity system control. Fuzzy logic has been applied in PAM control. To avoid mathematical parameter estimation, fuzzy logic was applied to model the inverse dynamics of PAM by obtaining input/output data from the system (Balasubramanian et al., 2005; Xie et al., 2011). The inverse dynamics model can be used to predict a feedforward pressure to eliminate tracking errors and achieve better overall stability (Balasubramanian et al., 2005). Hybrid controllers were developed, such as incorporating fuzzy logic with PID (Nuchkrua et al., 2013), incorporating fuzzy logic with sliding mode control (Chang et al., 2010) and incorporating fuzzy logic with neural network (Leephakpreeda et al., 2011). Self-organizing was used to modify fuzzy rules on-line (Chandrapal et al., 2010; Chang et al., 2010) to improve the ability of controller to handle the change of system dynamics.

This paper proposes a self-organizing fuzzy controller with model compensation to implement the position control of single PAM. First, an empirical model is established. Inspired by related work (Reynolds et al., 2003; Reynolds et al., 2003; Minh et al., 2010; Minh et al., 2011), this paper proposes a

novel empirical model which consists of hysteresis element, velocity dependent viscous damping element, rubber elasticity element that models the elastic force of rubber tube and contractile element that handles external load mounted on PAM in parallel, aiming to obtain an accurate model of PAM which is of simple form for control. Maxwell-slip elements (Minh et al., 2011) are adopted to model the hysteresis element. The time-variant character of rubber is small compared to the total hysteresis and becomes negligible at higher internal pressure and in the smaller length region (Minh et al., 2011). Therefore, it is not included in the proposed model.

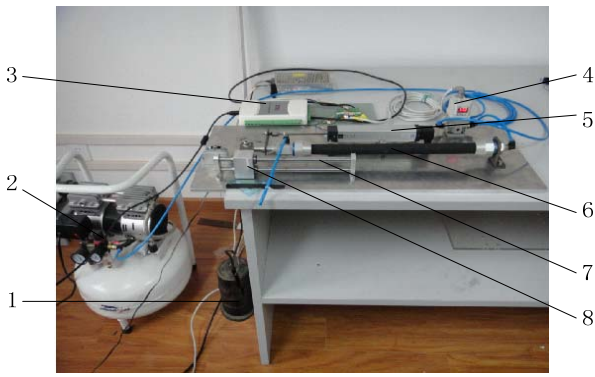
Damping can be divided into two categories, namely, stickiness damping which is related to position and viscous damping which is related to velocity. As the braided sheath and the rubber tube are mixed together in FESTO PAM, there is not kinetic friction between braided threads. The stickiness damping is mainly caused by the static friction between the braided sheath and the rubber tube which have relative movement trends during the extension and contraction of PAM. As found by some researchers (Chou et al., 1996; Tondu et al., 2000), hysteresis is velocity independent and history dependent, and is mainly caused by coulomb friction frictions in PAM. Therefore, hysteresis is adopted to model the stickiness damping caused by friction. Viscous damping in PAM is caused by the viscoelasticity of rubber. Viscous damping is the velocity dependent part of viscoelasticity. Rubber elasticity is the other part which is stress dependent. Viscous damping will be modeled by dynamic experiments while rubber elasticity will be derived by quasi-static experiment.

Then, a fuzzy controller is proposed for position control of single PAM. The proposed empirical PAM model is employed to produce a feed forward signal to reduce the creep of PAM caused by hysteresis and to improve the respond speed of the controller. To improve the robust of the controller, an on-line self-organizing mechanism is introduced to the controller.

The outline of this paper is as follow. Section 2 introduces the experiment setup. Section 3 derives the empirical model of PAM by experiments. Section 4 presents the controller design for position control of PAM. Section 5 gives experimental results and discussions. Conclusions are derived in Section 6.

## 2. EXPERIMENTAL SETUP

To obtain the hysteresis element and to implement close-loop position control of PAM, the length and the pressure inside PAM are needed. The length of PAM is measure by a displacement sensor. The pressure inside the PAM is measured by the pressure sensor inside the pneumatic proportional valve. PAM is in parallel with the displacement sensor and the guide rail as presented in Fig. 2. One end of the PAM is fixed on the platform by a bracket. The other end is fixed with a slider which moves along the guide rail. The load produced by weights is mounted on the moving end of PAM.



1–Load 2–Air source 3–Data acquisition card 4–Pneumatic proportional valve 5–Displacement sensor 6–PAM 7–Guide rail 8–Linear bearings

Fig. 2. Experiment setup.

The PAM is from FESTO (type MAS-20-400N) with a normal length of 400mm and a normal diameter of 20 mm. Its maximum contraction ratio is 25% and the maximum pressure permitted inside the PAM is 6 bars. The control valve (type ITV 2050-212N) is a voltage proportional valve from SMC and its maximum output pressure is 9 bars. The displacement sensor is from KTC with a linearity of  $\pm 0.05\%$ . The input signal is the position of PAM. The output control voltage and pressure of the solenoid valve are processed by data acquisition card (type USB7660) from ZTIC with 16-bit input channels and 12-bit output channels. Data acquisition card is controlled by PC. The GUI and control algorithm are developed with Visual C++. The GUI is shown in Fig. 3.

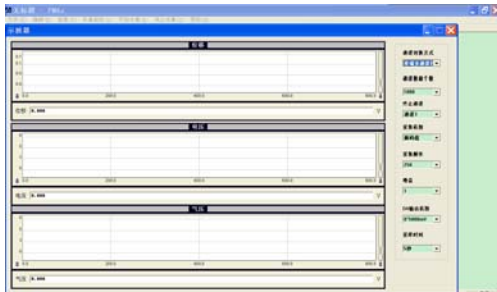


Fig. 3. The GUI of control software.

### 3. SYNTHETICAL MODEL OF PAM

In this section, hysteresis element, viscous damping element, rubber elasticity element and contractile element of PAM are modeled respectively and then synthesized. Finally, experiments are done to verify the accuracy of the proposed model. Rubber elasticity element is found to be a significant part of FESTO PAM model in this paper.

#### 3.1 Hysteresis element

Fig. 4 shows the pressure/contraction ratio of FESTO PAM without load. To avoid arousing the velocity dependent viscous damping, the experiment is done quasi statically with the pressure inside the rubber gradually increased. The contraction of PAM is shown by the upper half of every loop curve in Fig. 4, while the extension of PAM is shown by the

lower half of every loop curve. The maximum contraction ratio of FESTO PAM is 0.2583. Fig. 4 shows that the pressure inside the PAM at a contract ratio during extension is lower than that during contraction at the same contract ratio. The area of pressure/contraction loop in Fig. 4 is related to the amplitude of motion. This means that hysteresis in PAM is history dependent.

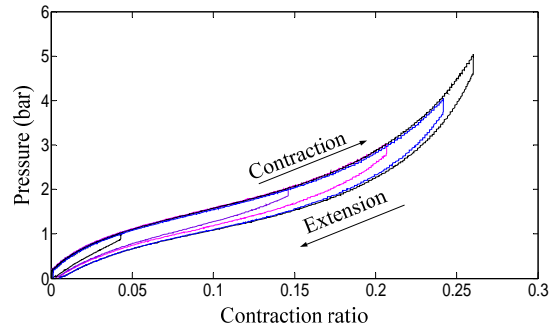


Fig. 4. Quasi-static pressure/position relationship of PAM.

Friction is assumed to cause hysteresis within PAM. In FESTO PAM, the braided sheath and the rubber tube are mixed together and do not move relatively, the friction between them is in a stage of presliding regime and thus is velocity independent but history dependent. This kind of friction can be well modeled by Maxwell element which is related to stiffness  $k$ , saturation force  $w$ , displacement  $x$  and friction force  $F$  (Lampaert et al., 2002) as shown in Fig. 5.a. Maxwell-slip model which was a lumped-parametric quasi-static model was adopted to capture the hysteresis in FESTO PAM (Minh et al., 2010; Minh et al., 2011). In Maxwell-slip model, several Maxwell-slip elements in parallel as shown in Fig. 5.b are used to describe the hysteresis of PAM.  $F_{hys\_out}$  is the total output.

However, the number of Maxwell-slip elements is intuitively selected. Minh et al. used four elements and found it was sufficient to model the PAM hysteresis (Minh et al., 2011).

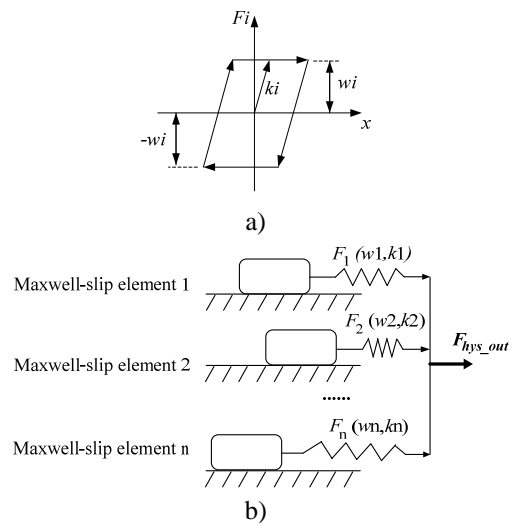


Fig. 5. a) Maxwell-slip element; b) Maxwell-slip model of PAM.

Hysteresis can be obtained by subtracting the free-moving measured data to the data from the constrained model (Minh et al., 2011). The FESTO PAM (MAS-20-400N) studied in this paper is different from that studied by Minh et al. (MAS-20-200N) only in length and the amplitude of the maximum pressure hysteresis in Fig. 4 is almost the same with that obtained by Minh et al. in Fig. 6 (0.51bars). Considering that the pressure hysteresis is related to the contraction ratio but the length of PAM, this paper employs the same Maxwell-slip elements as Minh et al. (Table 1) to model the hysteresis in FESTO PAM.

**Table 1. Parameters of Four Maxwell-slip Elements for PAM (Minh et al., 2011).**

Element	1	2	3	4
k	10	7.5	1.6	0.9
w	0.05	0.075	0.056	0.081

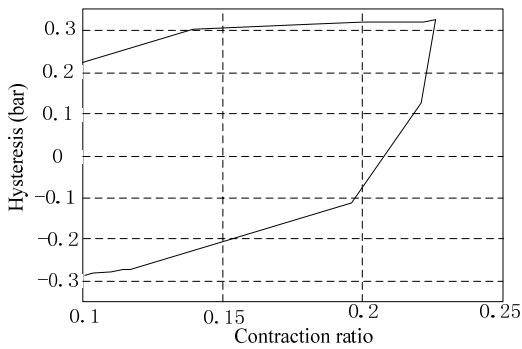


Fig. 6. Hysteresis in PAM (Minh et al., 2010).

3.2 Viscous damping element

To obtain the viscous damping in FESTO PAM, different speed to increase and decrease pressure inside PAM is tested. No load is mounted on PAM to get rid of the influence of load. Fig. 7 shows the pressure/position loop with different increase and decrease speed of pressure. The contraction of PAM is shown by the upper half of every loop curve, while the extension of PAM is shown by the lower half of every loop curve. The red loop is obtained by a quasi-static experiment. The contraction velocity and extension velocity for each loop increases from right to left. It is shown that with a faster contraction velocity the pressure at the same contraction ratio is higher. The viscous damping shows opposite direction to the move velocity during the contraction stage. With a faster moving velocity the pressure inside PAM is higher during extension as well. It seems that viscous damping does not change with the moving direction of PAM. Possible reason is that the velocity increase of PAM results in additional rubber elasticity due to the rubber identity. In this paper, the viscous damping is modeled by fitting data from experiment as shown in Fig. 8 derived from Fig. 7. A third-order polynomial is adopted to fit data in Fig. 8. The function of the fitted curve is

$$P_{vis} = 8.2913v^3 - 7.4333v^2 + 2.2167v + 0.039728 \quad (1)$$

where,  $P_{vis}$  is the pressure needed to overcome the viscous damping of PAM,  $v$  is the absolute velocity of PAM.

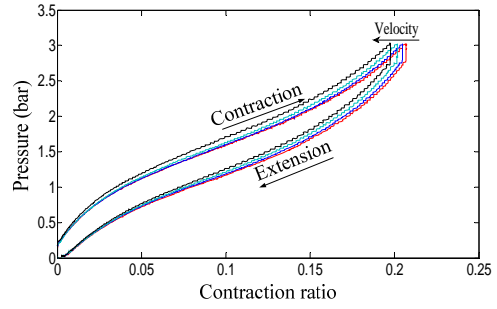


Fig. 7. Pressure/Position loop with different speed of pressure increase.

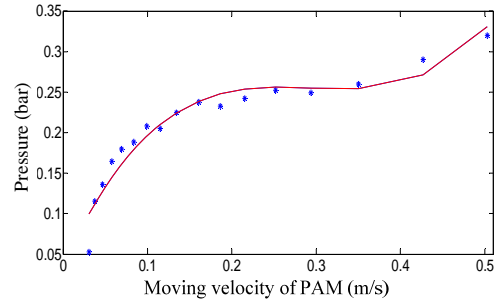


Fig. 8. Viscous damping element of PAM.

3.3 Rubber elasticity element

Rubber elasticity is obtained by subtracting the hysteresis element modeled in Section 3.1 from the quasi-static and no-load pressure/position curve with the largest stroke (contraction ratio: 0.258) in Fig. 4, as the quasi-static curve does not include viscous damping element and is convenient for data processing. The extracted rubber elasticity curve is shown by the blue lines in Fig. 9. There is some hysteresis shown by the two blue lines in Fig. 9. This may be due to the intuitive selection of Maxwell-slip elements. More Maxwell-slip elements can form a more sufficient hysteresis model of PAM. Compared with hysteresis element and viscous damping element, the rubber elasticity element is relatively large. In fact, pneumatic energy is transformed to the elastic energy in rubber of PAM. The average of the two blue lines is fitted by a third-order polynomial and can be expressed in function (2). The function of the red line in Fig. 4 is

$$P_e = 508.03\varepsilon^3 - 155.66\varepsilon^2 + 22.887\varepsilon \quad (2)$$

where  $P_e$  is the elasticity element and the unit is bar,  $\varepsilon$  is the contraction ratio of PAM.

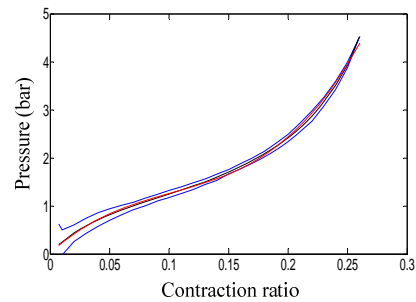


Fig. 9 Rubber elasticity element of PAM.

### 3.4 Contractile element

The contractile element is derived by using ideal PAM model based on principle of energy conservation (Chou et al., 1996). The contractile element can be written as

$$P_c = F / [\lambda(1-\varepsilon)^2 - b] \tag{3}$$

where  $P_c$  is the pressure needed to handle load on PAM,  $F$  is the load on the moving end of PAM,  $\varepsilon$  is the contraction ratio,  $\lambda = \frac{3\pi D_0^2}{4 \tan^2 \theta_0}$ ,  $b = \frac{\pi D_0^2}{4 \sin^2 \theta_0}$ ,  $D_0$  and  $\theta_0$  are the initial diameter and initial angle between braided threads respectively.

### 3.5 Model synthesis

Synthesizing the PAM hysteresis element, viscous damping element, rubber elasticity element and contractile element, the empirical model of PAM can be written as

$$P = P_{hys} + P_{vis} + P_e + P_c \tag{4}$$

where  $P$  is the pressure inside PAM.

### 3.6 Static discrepancy test of PAM model

Simple quasi-static and no-load experiments are used to investigate the accuracy of the proposed model. The experiments take two steps: (1) set the pressure inside PAM to a value calculated by using the proposed model at a reference PAM length; (2) the pressure is gradually adjusted to meet the reference PAM position accurately. The discrepancy between the proposed model and the real PAM is shown in Table 2. It is shown that there exist some discrepancy between the proposed model and the real PAM. The time-variant character of rubber, the intuitive selection of Maxwell-slip elements, and the friction between the guide rail and the linear bearing may be responsible for the discrepancy. However the discrepant pressure is small considering that the PAM in the experiments works at a pressure of approximately 2 bars.

**Table 2. Discrepancy of pressure inside PAM.**

Experiment number	Contraction ratio	Discrepant pressure (bar)
1	5%	0.12
2	7.5%	0.15
3	10%	0.20
4	12.5%	0.30

## 4. PAM CONTROLLER DESIGN

Fuzzy logic is a control strategy that uses expert experience and is widely applied to control system where the system model is difficult to establish. In this section, a self-organizing fuzzy controller with model compensation (SOFCMC) is proposed. The PAM model is used to create an

anticipated pressure inside the PAM. A self-organizing mechanism is employed to handle the uncertainties and variation of external load thus improves the robustness of the controller. The output of the controller is in an incremental way.

### 4.1 Fuzzification

The error ( $e$ ) and error rate ( $ec$ ) of PAM position are used as the input variable for the fuzzy logic controller. The input variable needs to be scaled to the fuzzy domain for  $e$  and  $ec$ . The scaling factor is chosen and optimized by experiment. The member function sets chosen for  $e$ ,  $ec$  and the output  $u$  are {NB, NM, NS, ZE, PS, PM, PB} and {NB, NM, NS, ZE, PS, PM, PB} respectively, where NB means Negative Big, NM means Negative Middle, NS means Negative Small, ZE means Zero, PS means Positive Small, PM means Positive Middle, PB means Positive Big. In this paper, NB is -3, NM is -2, NS is -1, ZE is 0, PS is 1, PM is 2, PB is 3. The fuzzy domain is shown in Fig. 10. Triangular membership functions are adopted for fuzzification.

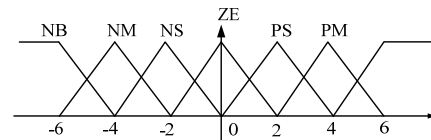


Fig. 10. Membership functions.

### 4.2 Fuzzy Rules

The fuzzy rules are in the following form:

$$\begin{aligned} \text{RULE}_i : & \text{If } e = A_i \text{ and } ec = B_j \\ & \text{then } u = r_{ij}, \quad i, j = 1, 2, \dots, 7 \end{aligned}$$

where  $A_i$ ,  $B_j$  and  $r_{ij}$  are member functions. The rules are shown in Table 3. There are totally  $7 \times 7 = 49$  rules in the fuzzy controller.

**Table 3. Fuzzy Rules.**

$e \backslash ec$	NB	NM	NS	NE	PS	PM	PB
NB	PB	PB	PM	PM	ZE	ZE	NS
NM	PB	PM	PM	PM	ZE	NS	NS
NS	PB	PM	PS	PS	ZE	NS	NM
ZE	PB	PM	PS	ZE	NS	NM	NB
PS	PM	PS	ZE	NS	NS	NM	NB
PM	PS	PS	ZE	NM	NM	NM	NB
PB	PS	ZE	ZE	NM	NM	NB	NB

### 4.3 Fuzzy Inference

The Mamdani min-min-max method shown in Fig. 11 is used for Fuzzy inference. The input variables  $e$  and  $ec$  have a membership for each fuzzy rule, the output depends on the smaller membership.

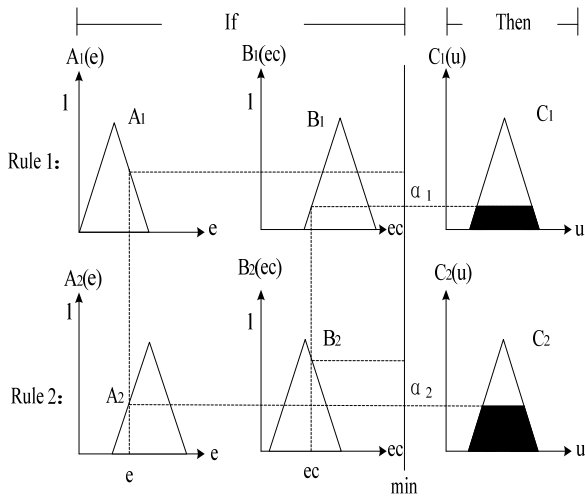


Fig. 11. Mamdani Fuzzy inference.

4.4 Self-organizing mechanism

A self-organizing mechanism is proposed in this section. Fuzzy rules in traditional fuzzy control cannot change while in self-organizing fuzzy controller the output of each rule is scaled to adapt to external load and disturbance. Thus the self-organizing mechanism improves the robustness of the control system.

The scaling factor for the  $i$  th fuzzy rule  $\alpha_{ik}$  at the  $k$  th sample time is as follows.

$$\alpha_{ik} = \alpha_{i(k-1)} + (1 - \zeta)e_{k-1} + \zeta ec_{k-1} \quad (6)$$

where  $e_{k-1}$ ,  $ec_{k-1}$  mean position error  $e$  and error rate  $ec$  at the  $(k-1)$  th sample time respectively,  $\zeta$  (0~1) is a weight value, in this paper  $\zeta = 0.2$ .

When the system experiences load variation or disturbance, the error of system grows bigger. In the self-organizing controller,  $\alpha_{ik}$  grows with error to increase the control output to handle with the load variation or disturbance.

4.5 Defuzzification

The Takagi-Sugeno-Kang method which uses a single fuzzy point as output member function instead of a distributed fuzzy set is used for the defuzzification. The output  $u_k$  at the sample time  $k$  is computed by the average weight of each rule.

$$u_k = u_{k-1} + \frac{\sum_{i=1}^{i=49} (1 + \alpha_{i(k-1)}) w_i r_i}{\sum_{i=1}^{i=49} w_i} \quad (5)$$

where  $w_i$  is the membership of each rule,  $\alpha_{i(k-1)}$  is the output scaling factor for rule  $i$  at sample time  $(k-1)$ .

As PAM is controlled by a voltage proportional solenoid valve,  $u_k$  is output as a voltage signal to the solenoid valve.

Incorporating self-organizing fuzzy logic and model compensation, the scheme of single PAM position controller is shown in Fig. 12 where  $r$  and  $y$  are the reference trajectory and the output trajectory,  $k1, k2$  are scaling factors.

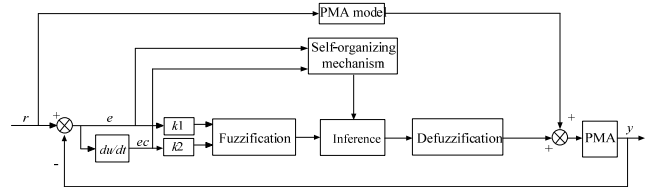


Fig. 12. Scheme of self-organizing fuzzy controller with model compensation (SOFCMC).

5. RESULTS AND DISCUSSIONS

The configuration of the experiment setup is presented in Fig. 2. Single PAM is tested to respond to step signal and sine signal. The load is applied to PAM by weights. Different loads are tested to verify the robustness of SOFCMC. PID controller and self-organizing fuzzy controller (SOFC) which doesn't include model compensation are tested to compare with SOFCMC.

The step response of PID, SOFC and SOFCMC is shown in Fig. 13. The rise time of the three controllers is show in Table 4. It is shown that, SOFCMC achieves the fastest response and PID achieves a faster response than SOFC. SOFC and SOFCMC cannot reach the reference position exactly due to the inherent characteristic of fuzzy controller. That is, when the input error is small enough, the output of the fuzzy controller is zero, thus the error cannot be eliminate completely. Therefore, small error results in a dead zone within fuzzy controller. The steady state error of SOFC and SOFCMC is within  $\pm 0.25\text{mm}$ .

Table 4. Rise time of step response

PID	1.67s
SOFC	3.28s
SOFCMC	0.87s

The performance of sine tracking of single PAM is illustrated in Fig. 14~17. It can be observed that SOFCMC shows the highest tracking accuracy among the three controllers while PID shows the lowest accuracy.

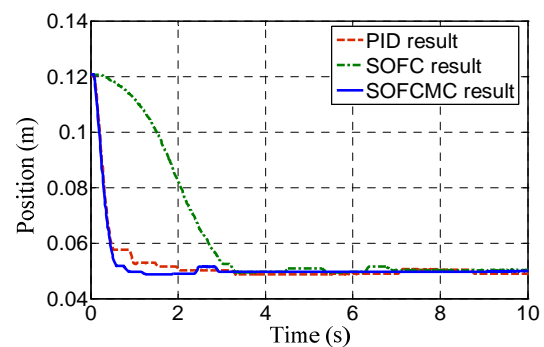


Fig. 13. Step response of PAM (load: 45N).

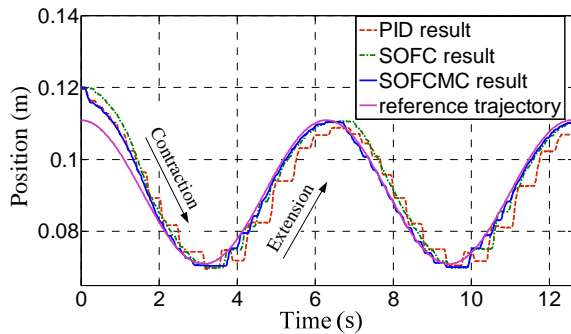


Fig. 14. Trajectory tracking of PAM (load: 45N).

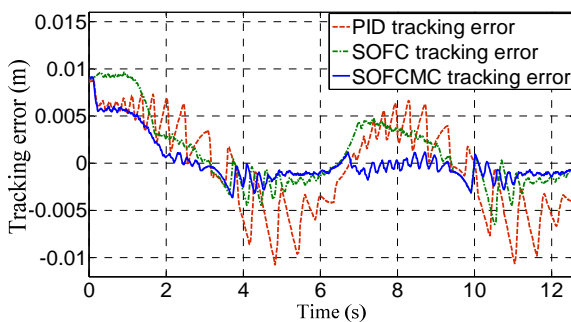


Fig. 15. Tracking error of PAM (load: 45N)

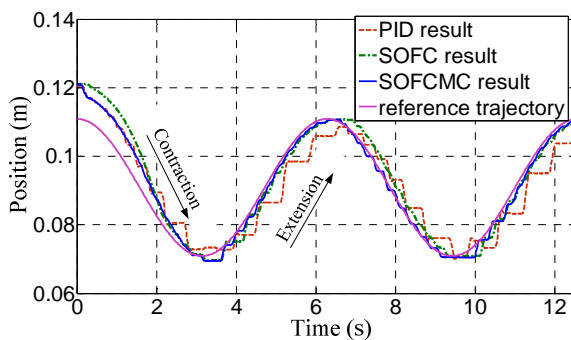


Fig. 16. Trajectory tracking of PAM (load: 85N).

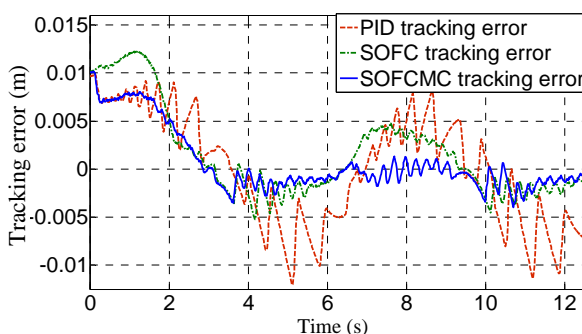


Fig. 17. Tracking error of PAM (load: 85N).

Fig. 14 and Fig. 16 show that the PAM creeps during trajectory tracking. To be specific, the PAM stops in a position and moves forward or backward suddenly. This phenomenon can be observed more obviously by the oscillation of tracking error in Fig. 15 and Fig. 17. The creep is the inherent characteristic of PAM caused mainly by the compliance of PAM. The compliance means that load

variations have a significant effect on position (Caldwell et al., 1995). To be specific, compliance of PAM is due to its small stiffness and low damper and thus the PAM will extend or contract over an equilibrium position when the load increases or decreases. Therefore, the variation of force acting on the end of PAM makes the tracking trajectory not so smooth and creep.

Comparing the oscillation during extension to that during contraction in Fig. 15 and Fig. 17, one can find that the creep of PAM during extension is generally more obvious than that during contraction. In fact, during the extension of PAM, the direction of load on PAM is the same as that of PAM motion, thus makes the creep of PAM more obvious. During the contraction of PAM, the direction of load on PAM is opposite to that of PAM motion and thus alleviates the creep. In Fig. 14 and Fig. 16, SOFCMC and SOFC show much better performance in restraining creep than PID controller generally. This suggests that fuzzy logic may be appropriate control strategy for PAM.

Amongst all the elements within PAM model, hysteresis element is the one which is most difficult to handle. This is because that hysteresis is related to the history of PAM and thus is very hard for controller without hysteresis compensation to adjust to the pressure to a desired one. With model compensation, the pressure needed to alleviate hysteresis is fed forward and eases the creep of PAM. From oscillation in Fig. 15 and Fig. 17, it can be found that SOFCMC shows an overall lower level of creep than SOFC. This indicates the effectiveness of model compensation, especially hysteresis compensation.

The static friction between the pull rod of the displacement sensor and its shell increases the creep. As PAM starts to move, it has to overcome this static friction. After the PAM overcomes the static friction, this friction switches to dynamic friction which is much smaller than static friction. Thus the PAM moves ahead suddenly. Feed a pressure forward based on friction model or reduce friction by improving the precision of the experimental apparatus could reduce creep to a lower level.

Comparing the reference trajectories and tracking results in Fig. 14~17, it can be found that the actual trajectories of PID and SOFC lag behind the reference trajectory. By adjust the parameters of PID and SOFC, the tracking results do not seem better than that. However, SOFCMC shows a much better performance of tracking the reference trajectories. This lag is caused by the ability of controller to output a proper voltage to the proportional solenoid valve in time. With model compensation, SOFCMC feeds forward a compensation pressure. This eliminates the dynamics of the system and alleviates the burden of the controller. Therefore, SOFCMC tracks the reference trajectory speedier and achieves better tracking performance.

The tracking error of SOFCMC is -3mm~1mm with a load of 45N shown in Fig. 15 and is -3.4mm~1mm with a load of 85N shown in Fig. 17. The tracking error of SOFCMC seems to change little with different load, thus verified its

robustness. SOFCMC also shows its ability to maintain the stability of system.

## 6. CONCLUSIONS

A novel empirical model of PAM is proposed to be used for control of single PAM in this paper. PAM is regarded as hysteresis element, viscous damping element, rubber elasticity element, contractile element in parallel. Experiments show that the model has a good agreement with actual PAM. A close-loop position control of PAM is performed. Due to the compliance of PAM and the variant load, PAM creeps during position tracking using PID. Compared with PID, SOFC and SOFCMC show much better performance. Thus fuzzy logic seems to be appropriate control strategies for PAM. SOFCMC achieves an overall lower level of creep than SOFC. This verifies the effectiveness of model compensation, especially hysteresis compensation. Moreover, with model compensation, SOFCMC significantly alleviates the trajectory lagging. To improve the robustness of the controller, a self-organizing mechanism is proposed. Experiment shows that the tracking error of SOFCMC changes slightly with different loads. This proves that the proposed controller is robust to the external load. The stability of SOFCMC is verified by experiments as well. Thus the proposed empirical model and self-organizing fuzzy logic controller based on it are appropriate for modeling and position control of single PAM. This will facilitate the application of PAMs in rehabilitation robot and other possible fields.

## 7. ACKNOWLEDGMENTS

This research is funded by National Natural Science Foundation of China (Grant No. 51475342).

## REFERENCES

- Balasubramanian, K. and Rattan, K. S. (2005). Trajectory tracking control of a pneumatic muscle system using fuzzy logic. *Annual Meeting of the North American Fuzzy Information Processing Society*, 472-477.
- Balasubramanian, S., Ward, J., Sugar, T. and He, J. (2007). Characterization of the dynamic properties of pneumatic muscle actuators. *IEEE 10th International Conference on Rehabilitation Robotics*, 764-770.
- Caldwell, D. G., Medrano-Cerda, G. A. and Goodwin, M. (1995). Control of pneumatic muscle actuators. *Control Systems, IEEE*, 15(1), 40-48.
- Carbonell, P., Jiang, Z.-P. and Repperger, D. (2001). Nonlinear control of a pneumatic muscle actuator: backstepping vs. sliding-mode. *Proceedings of the 2001 IEEE International Conference on Control Applications*, 167-172.
- Chandrapal, M., Chen, X. and Wang, W. (2010). Self organizing fuzzy control of pneumatic artificial muscle for active orthotic device. *Proceedings of the 6th annual IEEE Conference on Automation Science and Engineering*, 632-637.
- Chang, M.-K. (2010). An adaptive self-organizing fuzzy sliding mode controller for a 2-DOF rehabilitation robot actuated by pneumatic muscle actuators. *Control Engineering Practice*, 18(1), 13-22.
- Chou, C.-P. and Hannaford, B. (1996). Measurement and modeling of McKibben pneumatic artificial muscles. *IEEE Transactions on Robotics and Automation*, 12(1), 90-102.
- Doumit, M., Fahim, A. and Munro, M. (2009). Analytical modeling and experimental validation of the braided pneumatic muscle. *IEEE Transactions on Robotics*, 25(6), 1282-1291.
- Klute, G. K. and Hannaford, B. (2000). Accounting for elastic energy storage in McKibben artificial muscle actuators. *Journal of dynamic systems, measurement, and control*, 122(2), 386-388.
- Kothera, C. S., Jangid, M., Sirohi, J. and Wereley, N. M. (2009). Experimental characterization and static modeling of McKibben actuators. *Journal of Mechanical Design*, 131(9), 091010.
- Lampaert, V., Swevers, J. and Al-Bender, F. (2002). Modification of the Leuven integrated friction model structure. *IEEE Transactions on Automatic Control*, 47(4), 683-687.
- Leephakpreeda, T. (2011). Fuzzy logic based PWM control and neural controlled-variable estimation of pneumatic artificial muscle actuators. *Expert Systems with Applications*, 38(6), 7837-7850.
- Minh, T. V., Tjahjowidodo, T., Ramon, H. and Van Brussel, H. (2010). Cascade position control of a single pneumatic artificial muscle-mass system with hysteresis compensation. *Mechatronics*, 20(3), 402-414.
- Minh, T. V., Tjahjowidodo, T., Ramon, H. and Van Brussel, H. (2011). A new approach to modeling hysteresis in a pneumatic artificial muscle using the Maxwell-slip model. *IEEE/ASME Transactions on Mechatronics*, 16(1), 177-186.
- Nuchkrua, T. and Leephakpreeda, T. (2013). Fuzzy self-tuning PID control of hydrogen-driven pneumatic artificial muscle actuator. *Journal of Bionic Engineering*, 10(3), 329-340.
- Pujana-Arrese, A., Mendizabal, A., Arenas, J., Prestamero, R. and Landaluze, J. (2010). Modelling in Modelica and position control of a 1-DoF set-up powered by pneumatic muscles. *Mechatronics*, 20(5), 535-552.
- Repperger, D., Johnson, K. and Phillips, C. (1998). A VSC position tracking system involving a large scale pneumatic muscle actuator. *Proceedings of the 37th IEEE Conference on Decision and Control*, 4302-4307.
- Reynolds, D., Repperger, D., Phillips, C. and Bandry, G. (2003). Modeling the dynamic characteristics of pneumatic muscle. *Annals of Biomedical Engineering*, 31(3), 310-317.
- Rezoug, A., Tondu, B., Hamerlain, M. and Tadjine, M. (2013). Adaptive fuzzy nonsingular terminal sliding mode controller for robot manipulator actuated by pneumatic artificial muscles. *Proceeding of the IEEE International Conference on Robotics and Biomimetics*, 334-339.
- Shen, W. and Shi, G. (2011). An enhanced static mathematical model of braided fibre-reinforced pneumatic artificial muscles. *Proceedings of the*

- Institution of Mechanical Engineers, Part I: Journal of Systems and Control Engineering*, 225(2), 212-225.
- Shen, X. (2010). Nonlinear model-based control of pneumatic artificial muscle servo systems. *Control Engineering Practice*, 18(3), 311-317.
- Tondu, B. and Lopez, P. (2000). Modeling and control of McKibben artificial muscle robot actuators. *Control Systems, IEEE*, 20(2), 15-38.
- Tsagarakis, N. and Caldwell, D. G. (2000). Improved modelling and assessment of pneumatic muscle actuators. *Proceedings of the 2000 IEEE International Conference on Robotics and Automation*, 3641-3646
- Wickramatunge, K. C. and Leephakpreeda, T. (2013). Empirical modeling of dynamic behaviors of pneumatic artificial muscle actuators. *ISA Trans*, 52(6), 825-834.
- Xie, S. Q. and Jamwal, P. K. (2011). An iterative fuzzy controller for pneumatic muscle driven rehabilitation robot. *Expert Systems with Applications*, 38(7), 8128-8137.
- Xing, K., Huang, J., Wang, Y., Wu, J., Xu, Q. and He, J. (2010). Tracking control of pneumatic artificial muscle actuators based on sliding mode and non-linear disturbance observer. *IET control theory & applications*, 4(10), 2058-2070.
- Zhong, J., Fan, J., Zhu, Y., Zhao, J. and Zhai, W. (2014). Static Modeling for Commercial Braided Pneumatic Muscle Actuators. *Advances in Mechanical Engineering*, 2014, 1-6.